Two-dimensional MoS_2-enabled Flexible Rectenna for Wireless Energy Harvesting in the Wi-Fi Band

Xu Zhang[1], Jesús Grajal[2], José Luis Vázquez Roy[3], Ujwal Radhakrishna[1], Xiaoxue Wang[4], Winston Chern[1], Lin Zhou[1], Yuxuan Lin[1], Pin-Chun Shen[1], Xiang Ji[1], Xi Ling[5], Ahmad Zubair[1], Yuhao Zhang[1], Han Wang[6], Madan Dubey[7], Jing Kong[1], Mildred Dresselhaus[1,8], Tomás Palacios[1*]

[1]Department of Electrical Engineering and Computer Science, Massachusetts Institute of Technology, Cambridge, Massachusetts, 02139, USA

[2]Department of Signals, Systems and Radiocommunications, Universidad Politécnica de Madrid, Madrid, 28040, Spain

[3]Department of Signal Theory and Communications, University Carlos III of Madrid, Madrid, Spain.

[4] Department of Chemical Engineering, Massachusetts Institute of Technology, Cambridge, Massachusetts, 02139, USA

[5]Department of Chemistry, Boston University, Boston, Massachusetts, 02, USA

[6] Ming Hsieh Department of Electrical Engineering, University of Southern California, Los Angeles, California 90089, USA

[7] Army Research Laboratory, 2800 Powder Mill Road, Adelphi, Maryland, 20783, USA

[8]Department of Physics, Massachusetts Institute of Technology, Cambridge, Massachusetts, 02139, USA

*email: tpalacios@mit.edu

The unique mechanical and electronic properties of two-dimensional (2D) materials open up intriguing opportunities for flexible electronics[1,2,3]. Their atomic thickness and large-scale synthesis capability inspire a vision of "smart skin"[1,3–5], which could transform ordinary objects into an intelligent distributed sensor network[6]. However, although many important components of this new distributed electronic system have already been demonstrated (e.g. 2D materials-based transistors, sensors and memory devices[1,2,4,7]), a critical technological gap still remains: an efficient, flexible and always-on energy harvesting solution is indispensable, but still missing, to enable a self-powered system. Meanwhile the electromagnetic (EM) radiation from Wi-Fi systems operating at 2.4 GHz and 5.9 GHz[8] is becoming increasingly ubiquitous and it would be ideal to be able to harvest it to power future distributed electronics. However, the high frequencies used for Wi-Fi communications have remained elusive to all the RF harvesters (i.e. rectennas) made of flexible/large-area semiconductors[9–12]. Here we prototype an atomically thin and mechanically flexible MoS_2 semiconducting-metallic phase heterojunction-enabled rectenna with a cutoff frequency of 10 GHz, which represents roughly one order of magnitude improvement in speed compared with the current state-of-the-art for flexible electronics[9–12]. It is the first experimental demonstration of flexible rectifiers operating up to the X-band[8] and it covers most of the unlicensed industrial, scientific and medical (ISM) radio band, including the Wi-Fi channels. By integrating the ultrafast MoS_2 rectifier with a flexible Wi-Fi band antenna, we successfully fabricate the first fully flexible and integrated rectenna that demonstrates direct energy

harvesting of EM radiation in the Wi-Fi band with zero external bias (battery-free). Moreover, our MoS_2 rectifier also realizes successful frequency conversion as a flexible mixer beyond 10 GHz. This work provides a universal energy harvesting building block that can be integrated with various flexible electronic systems and paves the way towards using the existing Wi-Fi infrastructure as an energy hotspot for wireless charging future ubiquitous electronics.

Wireless power transmission dates back to Nikola Tesla's early work at the beginning of the twentieth century[13]. Efficient RF energy harvesters have been well-established on rigid substrates, such as silicon[14] and III-V compounds[15,16]. However, it has been extremely challenging to extend this technology into large-area, flexible electronic systems such as the ones that could be used in the future to monitor large infrastructure, or to enable truly ubiquitous sensing. This is in spite of the large variety of flexible semiconductors that have been investigated for this application. Organic semiconductors, such as pentacene, usually exhibit very low mobility (0.001-1 cm^2/Vs), which severely limits their performance in the gigahertz frequency range[17]. Metal oxides, such as amorphous indium gallium zinc oxide (IGZO), provide another option for flexible semiconductors. However, the cutoff frequency f_c of IGZO Schottky diodes as demonstrated on flexible plastic substrates is limited to about 1 GHz (f_c defined as the -3dB point as shown in the Methods section of this paper)[9,10,12]. Silicon microparticles in a polymer binder (SU8) have also been fabricated into flexible diodes exhibiting a cutoff frequency of 1.6 GHz[11]. However, the random distribution of particle sizes and distances results in a poor current on/off ratio and unreliable turn-on voltage, which deteriorates the rectification performance of the diode and the reliability for large-scale production. A comparison table summarizing the high frequency performance and solid-state properties of state-of-the-art flexible semiconductors can be found in the Extended Data Table S1. In addition, almost all the above methods use a vertical structure to increase the effective device area and thereby to reach high enough on-current I_{on}. However, in such a structure, the top and bottom electrodes of the diode inevitably form a parallel plate capacitor with large parasitic capacitance, which significantly hinders its high-speed applications. Lateral p-intrinsic-n (PIN) diodes made from single crystalline silicon[18] and germanium[19] nanomembranes can be fabricated on flexible substrates with 10 GHz performance. However, PIN diodes are usually limited to RF switches and power attenuators and are not applicable for energy harvesting[8]. Besides, the very high cost of single crystalline silicon and germanium nanomembranes and their materials and process complexity render them unfavorable for most practical applications.

Nowadays, Wi-Fi is becoming increasingly ubiquitous in both indoor and outdoor environments and provides an abundant source of always-on RF energy. It would be highly desirable if wearable electronics could directly harvest the radiation in the Wi-Fi band (2.4 GHz and 5.9 GHz) and thereby realize wireless charging. However, owing to the aforementioned challenges, a flexible RF rectifier that is fast enough to achieve wireless energy harvesting in the Wi-Fi band has not been demonstrated yet. In this work, we prototype an atomically thin and fully flexible MoS_2-based rectifier with a cutoff frequency of 10 GHz at zero external bias, using a facile self-aligned fabrication technique. By integrating with a Wi-Fi band

antenna, we demonstrated a fully flexible MoS_2-based battery-free rectenna (rectifying antenna) that can directly harvest Wi-Fi band (5.9 GHz) radiation on a plastic substrate.

MoS_2 is an emerging two-dimensional (2D) semiconductor with high mechanical robustness and with a demonstrated low-cost large-scale synthesis technology[2,20,21]. By patterning MoS_2 into a metallic-semiconducting (1T/1T'-2H) phase heterostructure[22] (Figure 1a), we demonstrated a lateral Schottky diode structure with a sub-10 fF junction capacitance. Together with a reduction in series resistance through self-aligned phase engineering, our MoS_2-based Schottky diode exhibits a cutoff frequency of 10 GHz (at zero bias, without de-embedding). This device is, to our knowledge, the first flexible rectifier with a cutoff frequency in the X-band, and it fully covers the global satellite positioning band (GPS, 1.58 GHz and 1.22 GHz), the cellular communication 4G long-term evolution band (LTE, 1.7 GHz and 1.9 GHz), the Bluetooth (2.4 GHz), the Wi-Fi channels (2.4 GHz and 5.9 GHz)[8], and even the next-generation 5G radio system. Moreover, with an intrinsic current responsivity up to 4.7 A/W, the performance of our 2D MoS_2 rectifier is comparable to the silicon-based Schottky diodes on rigid substrates[23]. By integrating this ultrafast flexible MoS_2–based rectifier with a flexible Wi-Fi band antenna, we demonstrate the first fully flexible and integrated Wi-Fi band rectenna that can directly harvest EM radiation in the Wi-Fi band with zero external bias (battery-free). This work can enable ubiquitous wireless charging for wearable and implantable medical sensors. We also demonstrate that our laterally designed MoS_2 diode can function as an RF mixer and successfully realize frequency conversion beyond 10 GHz. It is, to our knowledge, the highest performance MoS_2 mixer ever demonstrated on a flexible platform. This work provides critical building blocks for both wireless energy harvesting and wireless communication on flexible substrates. We also expect that the novel device architecture presented in this work could inspire new designs for other types of high-frequency devices to further improve their high-speed performance.

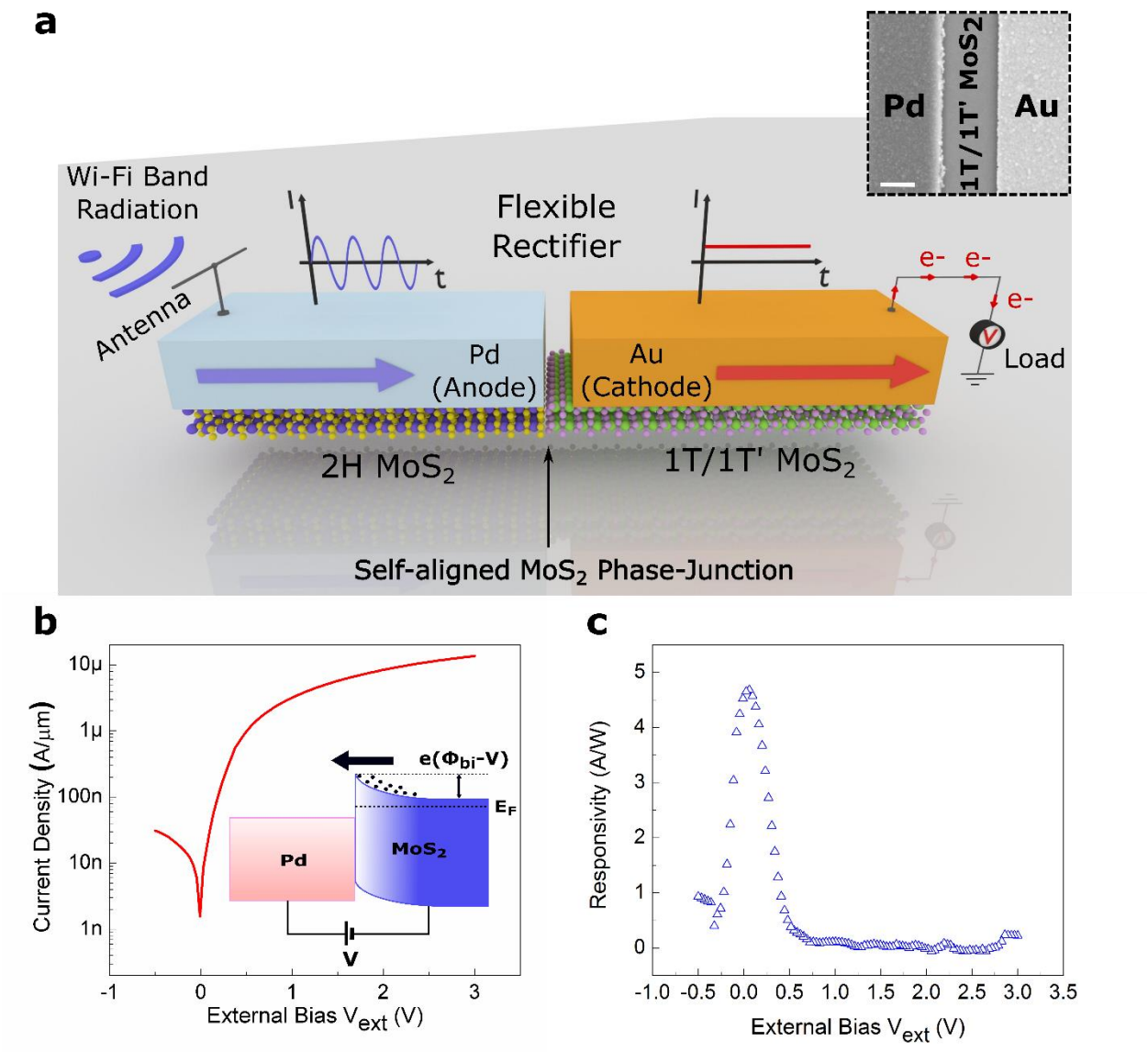

Figure 1 Flexible rectenna based on a two-dimensional self-aligned MoS_2 heterostructure-based Schottky diode. (a) Schematic of a lateral MoS_2 semiconducting-metallic (2H-1T/1T') phase-junction-based Schottky diode. The gold metal forms an Ohmic contact with metallic (1T/1T') MoS_2 and the metallic (1T/1T') MoS_2 also forms Ohmic contact with semiconducting (2H) MoS_2. The palladium metal forms Schottky contact with semiconducting (2H) MoS_2. The series resistance of the exposed channel region is minimized by converting semiconducting (2H) MoS_2 into metallic (1T/1T') MoS_2 in a self-aligned approach. The antenna converts the RF signal in the Wi-Fi band into an AC signal. The lateral MoS_2 diode is fast enough to rectify the AC signal and generate a DC signal to power a load at its output. Inset (upper right): SEM image of a MoS_2 Schottky rectifier. Scale bar: 1μm. The width of the MoS_2 diode is 40 μm. (b) The DC I-V characteristics of the MoS_2 Schottky diode in log scale. Inset: Band diagram of the MoS_2 Schottky junction under forward bias V. Φ_{bi} is the built-in potential of the MoS_2 Schottky diode. E_F indicates the Fermi level of the semiconducting (2H) phase MoS_2. (c) Current responsivity of the MoS_2 Schottky diode at different external bias points.

A rectenna is a passive electronic device that directly converts an incident electromagnetic (EM) wave into direct current (DC) and can provide power to a load connected to its output[23]. It consists of a receiver antenna (which converts the incoming EM wave into an alternating current (AC) signal) and a rectifying

circuit (which rectifies the AC signal to generate DC power). A particularly important figure-of-merit of high frequency Schottky diodes is their cutoff frequency f_c, above which the rectification will be very inefficient[8]. To first order, f_c is determined by the RC time constant of the diode[23]. In order to reduce the large parasitic capacitance in conventional vertical structures, here we propose an MoS_2 semiconducting-metallic (2H-1T/1T') phase-junction which enables a lateral Schottky diode with ultralow RC time constant. The device configuration and SEM image are illustrated in Figure 1a. The high work function metal Pd was selected to form a Schottky junction with the 2H semiconducting phase MoS_2. The exposed region of MoS_2 was chemically engineered into metallic (1T/1T') phase while the Pd metal contact served as a self-aligned mask to protect the 2H semiconducting phase region and to define a self-aligned MoS_2 semiconducting-metallic (2H-1T/1T') phase-junction (See Figure 1a and Methods). Subsequently, a layer of gold metal was deposited at high vacuum (10^{-8} Torr) to form an Ohmic contact with the metallic MoS_2 region[24]. The phase engineering of MoS_2 was investigated and confirmed by Raman spectroscopy, X-ray photoelectron spectroscopy (XPS) and transport studies (Extended Data Figure S1 and Figure S2). The contact between 1T/1T' MoS_2 and 2H MoS_2 was confirmed to be Ohmic contact and its contact resistance was obtained by transfer length method (TLM) (Extended Data Figure S3). Therefore, the Schottky junction between Pd and 2H MoS_2 is the dominating source of nonlinearity for rectification. The self-aligned metallic phase region of MoS_2 is the key to reduce the series resistance of the MoS_2 Schottky diode. Meanwhile, such a lateral configuration, together with the atomic thickness of the channel region, significantly minimizes the capacitance of the device.

Figure 1b shows the quasi-static I-V characteristics of the MoS_2 Schottky diode. The band alignment of the MoS_2 Schottky junction can be found in the inset of Figure 1b. The nonlinearity of the MoS_2 diode I-V characteristics plays a key role in the fundamental process of rectification. The current responsivity of a nonlinear rectifier provides a measure of the rectified DC output current for a given input RF power[8]. It can be calculated as (see Methods)

$$R_i = \frac{\left.\frac{d^2 I}{dV^2}\right|_{V=V_0}}{2 \cdot \left.\frac{dI}{dV}\right|_{V=V_0}} \quad , \qquad (2)$$

where V_0 is the operating bias point. As shown in Figure 1c, the current responsivity of the MoS_2 Schottky diode around zero bias is about 4.7 A/W, which is comparable to rigid silicon devices[23].

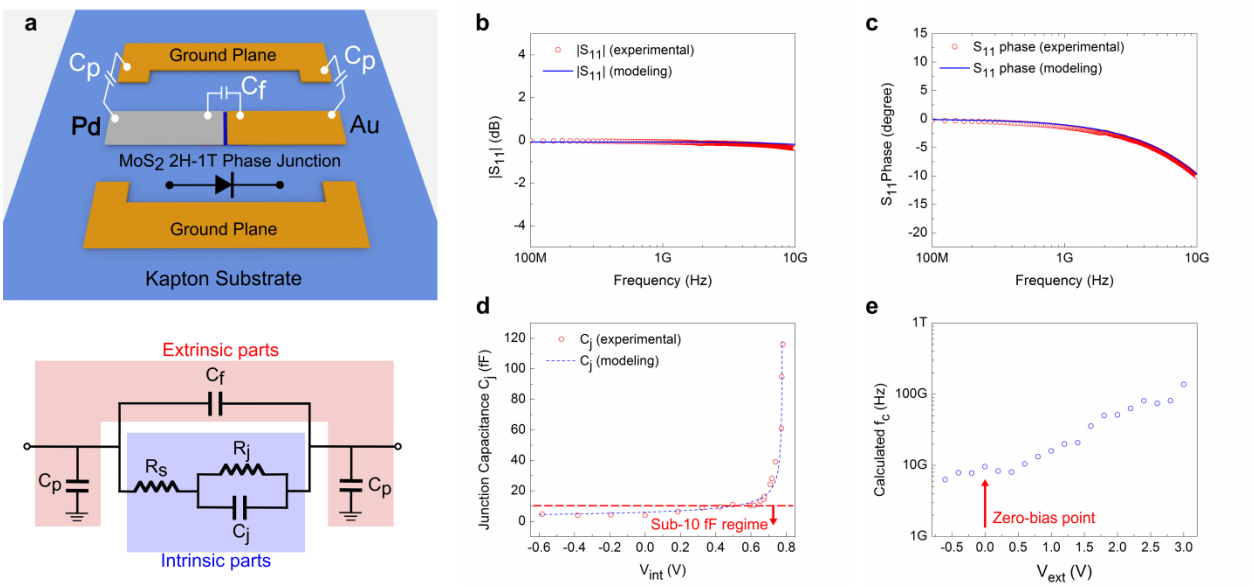

Figure 2 S-parameter measurements and equivalent circuit modeling of the flexible MoS_2 rectifier. (a) Top: The G-S-G coplanar configuration for S-parameter measurements. Schematic of the origin of the fringing capacitance C_f (the capacitance between the anode and cathode metal pads) and parasitic capacitance C_p (the capacitance between the electrodes of the diode and the ground plane). Bottom: Equivalent circuit of the MoS_2 Schottky rectifier, including both intrinsic components (R_s, R_j and C_j) and extrinsic parasitic components (C_f and C_p). (b)(c) The magnitude and phase of S_{11}. Blue line: Modeling data based on the equivalent circuit in Figure 2a. Red open circles: Experimental data from S-parameter measurements. (d) The junction capacitance C_j obtained from S-parameter. Red open circles: experimental data from S-parameter. Blue dash line: modeling data based on $C_j = C_0/\sqrt{1 - V/\Phi_{bi}}$. (e) Calculated cutoff frequency f_c based on R_s, R_j and C_j under different biasing conditions.

In order to study the high frequency performance of our lateral MoS_2 Schottky diode, we carried out scattering parameter (S-parameter) measurements by using a vector network analyzer (Keysight N5230A). A coplanar transmission line and a ground-signal-ground (G-S-G) probe configuration (Figure 2a top) were used to characterize the device at high frequencies[8]. We built an equivalent circuit to model the MoS_2 Schottky diode (Figure 2a bottom and Methods). Figure 2b and Figure 2c compare the modeled and measured data of the magnitude and phase of S_{11}, respectively. It can be found that the modeling result based on Figure 2a equivalent circuit matches the experimental S-parameter result fairly well. (The modeling and experimental results of S_{21} and S_{22} are summarized in Extended Data Figure S4). The S-parameter measurement allows us to obtain the resistive and capacitive components of the phase-engineered MoS_2 Schottky diode. Figure 2d summarizes the evolution of junction capacitance C_j at different internal biases. The internal bias V_{int} is the voltage dropped across the nonlinear junction resistance R_j only, and it can be calculated as $V_{int} = V_{ext} - I \cdot R_s$, where V_{ext} is the total bias applied across the MoS_2 diode and R_s is the series resistance of the MoS_2 Schottky diode. The junction capacitance of a Schottky diode can be modeled by[25]

$$C_j = \frac{C_0}{\sqrt{1-\frac{V}{\Phi_{bi}}}} \quad (3)$$

As shown in Figure 2d, the experimental C_j follows well the above expression (3). In the low-bias region (V<0.4V), the junction capacitance C_j of the MoS_2 diode is in the sub-10 fF regime (device width: 40μm), which is at least one order of magnitude lower than state-of-the-art flexible rectifiers[9–12]. The series resistance R_s and junction resistance R_j are also extracted and analyzed (Extended Data Figure S5 and Methods). These results are further confirmed by quasi-static IV measurement and modeling (Extended Data Figure S6). The fringing capacitance C_f and parasitic capacitance C_p are obtained to be about 10 fF and 20 fF, respectively, from S-parameter measurements. This result is also consistent with C-V measurements (See Extended Data Figure S7 and analysis in Methods).

We note that not all of the incident RF power absorbed by the MoS_2 Schottky diode is consumed by the nonlinear junction resistance R_j. Part of the RF power will be dissipated in the series resistance R_s. The portion of RF power absorbed by R_j will decrease as the operating frequency rises (see analysis in Methods). Conventionally, the cutoff frequency of a Schottky diode is defined as the frequency at which P_j/P_{RF} drops by ½ compared with the value at DC (also known as the "-3dB point")[8,26], where P_j is the power absorbed in the nonlinear R_j of the diode and P_{RF} is the total power absorbed by the diode. A simple analysis leads to the following expression for the cutoff frequency (Methods)[26]:

$$f_c = \frac{\sqrt{1+\frac{R_j}{R_s}}}{2\pi R_j C_j} \quad (4)$$

The cutoff frequency of our MoS_2 diode at different biases is calculated and illustrated in Figure 2e. At zero bias, a cutoff frequency around 10 GHz is expected. In the next section it will be further experimentally examined. Since we are targeting battery-free applications of the MoS_2-based rectenna in this work, we only focus on its zero-bias operation.

As a system-level demonstrator, we built a single-stage flexible MoS_2-based RF energy harvesting circuit. The circuit diagram can be found in Extended Data Figure S8. The circuit was first tested by generating an input RF signal through a signal generator (Keysight N5183A) and connecting it directly to the input of the MoS_2 rectifier. The rectified output voltage V_{out} was then measured using an oscilloscope with 1 MΩ impedance, which is in shunt with a load resistance. (see Methods). The optimum load resistance was found to be about 10 kΩ. Figure 3a shows output voltage V_{out} as a function of delivered RF power P_{RF} (*i.e.* the power absorbed by the MoS_2 diode) at different frequencies. As expected, the rectified voltage V_{out} increases as the RF power fed into the diode increases. In the Wi-Fi band (2.4 GHz and 5.9 GHz), we calculated the RF-DC power conversion efficiency, which is defined as the ratio between the output DC power ($P_{DC} = V_{out}^2/R_L$) and the input delivered RF power P_{RF}, i.e. $\eta = P_{DC}/P_{RF}$ (Figure 3b). At 2.4 GHz, the

maximum power efficiency η_{max} can reach 40.1% at input power of -0.7 dBm. The results are also benchmarked with the state-of-the-art rigid technology (Si and GaAs Schottky diodes) at the same frequency and the same input power level (see Extended Data Figure S9). As shown in Figure 3c, at a delivered RF power of ~ 5 mW, an output voltage of 3.5 V can be achieved. V_{out} drops as the input RF signal frequency increases. Our flexible MoS_2 Schottky diode exhibits a cutoff frequency of 10 GHz (using the -3 dB point definition), which is high enough to cover both of the commonly used Wi-Fi channels (2.4 GHz and 5.9 GHz).

We integrated the MoS_2 rectifier with a flexible receiver antenna fabricated on the same piece of flexible Kapton film (Figure 3d). The optical image of the MoS_2 rectenna is shown in Figure 3e. The antenna was designed to have a center frequency at the 5.9 GHz Wi-Fi channel (IEEE 802.11 standards). The fabrication process can be found in the Methods section and Extended Data Figure S10, while the EM simulation and characterization of the flexible 5.9 GHz antenna can be found in the Extended Data Figure S11. In order to test the entire harvesting system, we approached a commercial Wi-Fi band transmitter antenna (powered by signal generator, input power: ~2mW) to the integrated MoS_2 rectenna. The flexible MoS_2 rectenna was successful in wirelessly harvesting the RF power in the Wi-Fi channel (5.9 GHz) and generate a rectified output voltage up to 250 mV (distance from transmitter antenna: ~2.5 cm). This was achieved even without properly matching the impedance between the antenna and the MoS_2 rectifier (*i.e.* the actual delivered power to the MoS_2 rectifier is only a fraction of the available input power). We anticipate that the efficiency of the energy harvesting circuit can be significantly increased through a joint optimization of the antenna and circuit impedance matching by incorporating printed passive components[27]. With the demonstrated record-high cutoff frequency (10 GHz) fully covering the Wi-Fi and cellular band, combined with a full integration on flexible Kapton substrates, our phase-engineered MoS_2 Schottky diode enables the first experimental demonstration of a flexible rectenna as an RF energy harvester operating in the Wi-Fi band (IEEE 802.11 standards). It also provides a novel device architecture that could be promising towards ambient Wi-Fi and cellular energy harvesting in the future (detailed analysis see Methods). Meanwhile we also note that the ultimate flexible wireless energy harvesting of ambient Wi-Fi band energy requires continuous optimization in the material engineering (in particular, reducing series resistance by optimizing the phase change process), matching circuit and antenna design.

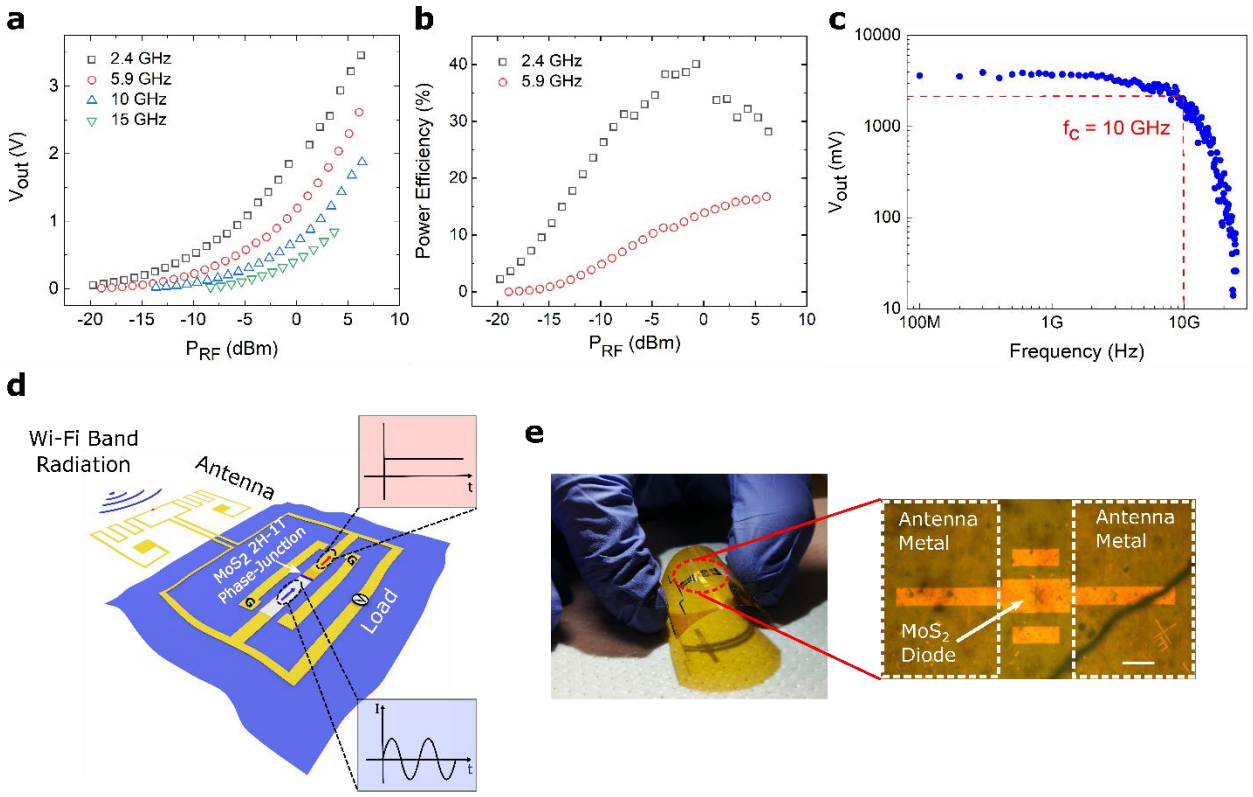

Figure 3 Demonstration of the MoS_2 phase-junction-enabled rectenna as a wireless RF energy harvester (a) The output voltage as a function of the input power delivered to the device at four different frequencies (2.4 GHz, 5.9 GHz, 10 GHz, 15 GHz). Circuit diagram can be found in Extended Data Figure S8. (b) The power efficiency of MoS_2 rectifiers as a function of the input power delivered to the device in the Wi-Fi band. (c) Output voltage as a function of frequency of the input signal for P_{RF} = 5 mW. The Wi-Fi bands are also indicated in the figure. The cutoff frequency of 10 GHz is high enough to fully cover the Wi-Fi bands (IEEE 802.11 standards). (d) Illustration of a flexible MoS_2 phase-junction-based rectifier integrated with a flexible Wi-Fi band antenna for wireless energy harvesting. The Wi-Fi band AC signal from the antenna is rectified into DC signal by the ultrafast MoS_2 rectifier. (e) Picture of a fully flexible and integrated MoS_2 rectenna on a flexible Kapton substrate. The region of MoS_2 rectifier is zoomed in (right panel). Scale bar: 100 μm.

In order to further demonstrate the high frequency performance of the MoS_2 phase-junction-enabled diode, we also built flexible frequency mixers on Kapton films. Frequency conversion and mixing are key building blocks of any modern wireless communication system. A mixer based upon the nonlinear I-V characteristics of the MoS_2 diode produces an output signal with frequency components at the sum and difference of its two input signals. One of the input signals is typically a local oscillator with frequency f_{LO} and the other signal is the RF carrier with a frequency f_{RF}[8] (Figure 4a). Thanks to the high-speed performance of our MoS_2 Schottky diode, we successfully demonstrated a flexible single-ended RF mixer on a Kapton substrate to realize both frequency up-conversion and down-conversion beyond 10 GHz. As shown in Figure 4b, a local oscillator f_{LO} = 8 GHz and an RF carrier signal at f_{RF} = 10.4 GHz were combined and fed into the MoS_2 diode. At its output, both the up-converted frequency at $f_{RF} + f_{LO}$ = 18.4 GHz and the down-converted frequency at $f_{RF} - f_{LO}$ = 2.4 GHz were detected by a spectrum analyzer (Keysight N9020A). When f_{LO} = 1 GHz and f_{RF} = 1.4 GHz were mixed through the MoS_2 Schottky diode, the

intermediate frequencies at $f_{IF} = f_{RF} + f_{LO}$ = 2.4 GHz and $f_{IF} = f_{RF} - f_{LO}$ =0.4 GHz were detected (Figure 4c). The conversion loss and 1dB compression point are shown in the Extended Data Figure S12. The high frequency performance of the flexible MoS_2 mixers can be further improved by improving the impedance matching, which is not optimized in this proof-of-concept demonstration. We note that, although a 42 GHz cutoff frequency has been claimed in MoS_2 transistors on rigid substrates[28,29] for amplifier applications, to the best of our knowledge, this work is the first experimental demonstration of a flexible MoS_2-based mixer beyond 10 GHz. This MoS_2-based mixer is also advantageous over graphene-based mixers[30] in terms of system-level monolithic integration since semiconducting MoS_2 can also enable other building blocks such as digital/logic[4] circuits and energy harvesting on a flexible platform.

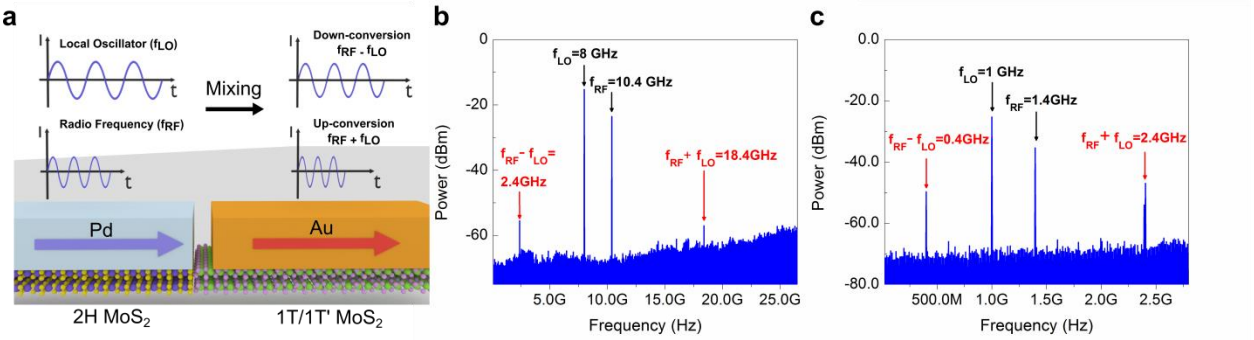

Figure 4 Demonstration of the MoS_2 diode-based mixer operating in the gigahertz range. The output signals are measured by a spectrum analyzer (Keysight N9020A) with an input impedance of 50 Ω. (a) Illustration of the frequency conversion of an RF mixer with two inputs: an RF carrier frequency at f_{RF} and a local oscillator frequency f_{LO}. At its output, $f_{IF} = f_{RF} \pm f_{LO}$ can be generated. (b) Experimental demonstration of the frequency conversion of a MoS_2-based GHz mixer. The radio frequency f_{RF} = 10.4 GHz. The local oscillator f_{LO} = 8 GHz. The down-converted intermediate frequency f_{IF} = 2.4 GHz. The up-converted intermediate frequency f_{IF} = 18.4 GHz. (c) Experimental demonstration of the frequency conversion of a MoS_2-based GHz mixer. The radio frequency f_{RF} = 1.4 GHz. The local oscillator f_{LO} = 1 GHz. The down-converted intermediate frequency f_{IF} = 0.4 GHz. The up-converted intermediate frequency f_{IF} = 2.4 GHz.

In summary, we describe the design, fabrication and testing of an atomically thin and flexible MoS_2 phase-heterostructure-enabled ultrafast Schottky diode with a cutoff frequency of 10 GHz (with zero external bias). The MoS_2 semiconducting-metallic lateral phase heterostructure-based diode exhibits a sub-10 fF capacitance which is one order of magnitude smaller than state-of-the-art flexible rectifiers. The self-aligned phase heterostructure also allows a significant and simultaneous reduction in series resistance. A large improvement in the RC time constant enables the first experimental demonstration of flexible high-speed rectifiers with operation frequency fully covering the Wi-Fi bands. By integrating the MoS_2 rectifier with a flexible Wi-Fi band antenna, we successfully demonstrate the first fully flexible and integrated rectenna that can wirelessly harvest the electromagnetic (EM) radiation in the Wi-Fi band. The MoS_2 rectenna can operate at zero external bias, which makes it a battery-free device and will be particularly useful for energy harvesting applications. Frequency conversion beyond 10 GHz is also demonstrated by using this self-aligned flexible MoS_2 phase-heterostructure-based diode.

References

1. Fiori, G. *et al.* Electronics based on two-dimensional materials. *Nat. Nanotechnol.* **9,** 768–779 (2014).
2. Wang, Q. H., Kalantar-Zadeh, K., Kis, A., Coleman, J. N. & Strano, M. S. Electronics and optoelectronics of two-dimensional transition metal dichalcogenides. *Nat. Nanotechnol.* **7,** 699–712 (2012).
3. Akinwande, D., Petrone, N. & Hone, J. Two-dimensional flexible nanoelectronics. *Nat. Commun.* **5,** 5678 (2014).
4. Chhowalla, M., Jena, D. & Zhang, H. Two-dimensional semiconductors for transistors. *Nat. Rev. Mater.* **1,** 16052 (2016).
5. Mak, K. F. & Shan, J. Photonics and optoelectronics of 2D semiconductor transition metal dichalcogenides. *Nat. Photonics* **10,** 216–226 (2016).
6. Dargie, W. & Poellabauer, C. *Fundamentals of Wireless Sensor Networks: Theory and Practice*. (John Wiley & Sons, Ltd, 2010). doi:10.1002/9780470666388
7. Jariwala, D., Sangwan, V. K., Lauhon, L. J., Marks, T. J. & Hersam, M. C. Emerging Device Applications for Semiconducting Two-Dimensional Transition Metal Dichalcogenides. *ACS Nano* **8,** 1102–1120 (2014).
8. Pozar, D. *Microwave Engineering, 4th Edition*. (2012).
9. Chasin, A. *et al.* An Integrated a-IGZO UHF Energy Harvester for Passive RFID Tags. *IEEE Trans. Electron Devices* **61,** 3289–3295 (2014).
10. Chasin, A. *et al.* UHF IGZO Schottky diode. in *2012 International Electron Devices Meeting* 12.4.1-12.4.4 (2012).
11. Sani, N. *et al.* All-printed diode operating at 1.6 GHz. *Proc. Natl. Acad. Sci.* **111,** 11943–11948 (2014).
12. Zhang, J. *et al.* Flexible indium–gallium–zinc–oxide Schottky diode operating beyond 2.45 GHz. *Nat. Commun.* **6,** 7561 (2015).
13. Tesla, N. Apparatus for utilizing effects transmitted from a distance to a receiving device through natural media. (1901).
14. Strohm, K. M., Buechler, J. & Kasper, E. SIMMWIC rectennas on high-resistivity silicon and CMOS compatibility. *IEEE Trans. Microw. Theory Tech.* **46,** 669–676 (1998).

15. Suh, Y.-H. & Chang, K. A high-efficiency dual-frequency rectenna for 2.45- and 5.8-GHz wireless power transmission. *IEEE Trans. Microw. Theory Tech.* **50,** 1784–1789 (2002).
16. Sizov, F. & Rogalski, A. THz detectors. *Prog. Quantum Electron.* **34,** 278–347 (2010).
17. Steudel, S. *et al.* Ultra-High Frequency rectification using organic diodes. in *2008 IEEE International Electron Devices Meeting* 1–4 (2008). doi:10.1109/IEDM.2008.4796622
18. Seo, J.-H. *et al.* Investigation of various mechanical bending strains on characteristics of flexible monocrystalline silicon nanomembrane diodes on a plastic substrate. *Microelectron. Eng.* **110,** 40–43 (2013).
19. Qin, G. *et al.* Fabrication and Characterization of Flexible Microwave Single-Crystal Germanium Nanomembrane Diodes on a Plastic Substrate. *IEEE Electron Device Lett.* **34,** 160–162 (2013).
20. Hsu, A. *et al.* Large-Area 2-D Electronics: Materials, Technology, and Devices. *Proc. IEEE* **101,** 1638–1652 (2013).
21. Lee, Y.-H. *et al.* Synthesis of Large-Area MoS2 Atomic Layers with Chemical Vapor Deposition. *Adv. Mater.* **24,** 2320–2325 (2012).
22. Kappera, R. *et al.* Phase-engineered low-resistance contacts for ultrathin MoS2 transistors. *Nat. Mater.* **13,** 1128–1134 (2014).
23. Donchev, E. *et al.* The rectenna device: From theory to practice (a review). *MRS Energy Amp Sustain.- Rev. J.* **1,** (2014).
24. English, C. D., Shine, G., Dorgan, V. E., Saraswat, K. C. & Pop, E. Improved Contacts to MoS2 Transistors by Ultra-High Vacuum Metal Deposition. *Nano Lett.* **16,** 3824–3830 (2016).
25. Sze, S. M. & Ng, K. K. *Physics of Semiconductor Devices*. (Wiley, 2007).
26. Cowley, A. M. & Sorensen, H. O. Quantitative Comparison of Solid-State Microwave Detectors. *IEEE Trans. Microw. Theory Tech.* **14,** 588–602 (1966).
27. Zhou, N., Liu, C., Lewis, J. A. & Ham, D. Gigahertz Electromagnetic Structures via Direct Ink Writing for Radio-Frequency Oscillator and Transmitter Applications. *Adv. Mater.* **29,** 1605198 (2017).
28. Park, S. *et al.* High-frequency prospects of 2D nanomaterials for flexible nanoelectronics from baseband to sub-THz devices. in *2015 IEEE International Electron Devices Meeting (IEDM)* 32.1.1-32.1.4 (2015).

29. Cheng, R. *et al.* Few-layer molybdenum disulfide transistors and circuits for high-speed flexible electronics. *Nat. Commun.* **5,** 5143 (2014).

30. Wang, H., Hsu, A., Wu, J., Kong, J. & Palacios, T. Graphene-Based Ambipolar RF Mixers. *IEEE ELECTRON DEVICE Lett.* **31,** 906–908 (2010).

Acknowledgements This work was financially supported by the Army Research Laboratory (Grant W911NF-14-2-0102), the STC Center for Integrated Quantum Materials (NSF Grant No. DMR-1231319), the Air Force Office of Scientific Research under the MURI-FATE program (Grant No. FA9550-15-1-0514) and National Science Foundation Grant DMR-1507806. Device fabrication was carried out at the MIT Microsystems Technology Laboratories. X-ray spectroscopy studies were done in the Cornell Center for Materials Research Shared Facilities. We acknowledge Prof. Karen Gleason and Dr. Amir Nourbakhsh for discussions.

Author Contributions X.Z. and T.P. conceived and designed the experiments. X.Z. fabricated the flexible devices. J.G., X.Z. and U. R. carried out the high frequency measurements. X.Z. and J.G. did the circuit modeling and data analysis. X.W. and X.Z. performed the chemical phase change of MoS_2 samples. X.Z., X.W. and L.Z. did the spectroscopic study. W.C. and X.Z. did the CV measurement. J.L.V.R. and J.G. designed and fabricated the flexible antenna. All authors provided constructive comments on the manuscript.

Author Information The authors declare no competing financial interests. Readers are welcome to comment on the online version of the paper. Correspondence and requests for materials should be addressed to T.P. (tpalacios@mit.edu).

Methods

Rectenna Fabrication and Integration

We fabricated flexible high-speed rectifiers based on MoS_2 semiconducting-metallic (2H-1T/1T') phase-junctions. Few-layer MoS_2 was obtained by the exfoliation method from bulk crystals. All the fabrication was done on flexible DuPont Kapton polyimide films with 50.8 μm thickness. E-beam lithography (EBL) with PMMA (*poly(methyl methacrylate)*) as e-beam resist was used to define the Schottky contact region on semiconducting (2H) MoS_2. In order to avoid charging effects on the insulating Kapton substrate during electron beam lithography (EBL), we coated a layer of conductive liquid ESPACER (purchased from Showa Denko) on PMMA as a charge dissipating agent. After EBL exposure, the ESPACER was rinsed off by distilled water before the development of the PMMA resist. Then 50 nm Palladium (Pd) was deposited to form a Schottky contact with MoS_2 by e-beam evaporation. After the formation of the Schottky contact, the Kapton film with the Pd/MoS_2 structure was immersed into 1.6 M n-Butyllithium (from Sigma Aldrich) solution for 10 minutes to convert the exposed region of the MoS_2 into the metallic phase[22]. This process was done in the N_2 atmosphere of a glove box. XPS and Raman spectroscopy were carried out to confirm the phase transition of MoS_2 (Extended Data Figure S1). The 1T phase MoS_2 is metastable under ambient condition, and part of the 1T region will convert into 1T' phase. However, the 1T/1T' mixture MoS_2 remains metallic IV characteristics even after baking (180 ˚C for 3 min) (See Extended Data Figure S2). The Pd metal contact served as a self-aligned mask to protect the 2H semiconducting region of MoS_2 lying underneath. Then the Kapton film was rinsed by hexane thoroughly to remove any lithium residue. A second EBL process was performed to define the Ohmic contact region with the phase-engineered MoS_2. Then 50 nm gold (Au) was deposited by e-beam evaporation in high vacuum (10^{-8} Torr) to form Ohmic contact with MoS_2. Finally, the coplanar transmission line (G-S-G) structure (5nm Ti/50nm Au) was fabricated by EBL for high frequency S-parameter measurements. This RC time constant reduction, due to self-aligned phase engineering and lateral structure, is largely immune to the partial 1T to 1T' phase conversion. Our MoS_2 rectenna can stably operate under ambient condition and we found its reliable operation can last for at least one year without noticeable degradation.

The Wi-Fi band receiver antenna was designed using CST microwave studio. The flexible antenna was fabricated by e-beam evaporation of 5 nm Ti/70 nm Au on a 50.8 μm Kapton thin film. The EM simulation and S-parameter measurements of the flexible antenna are shown in Extended Data Figure S11. Its center frequency is about 5.9 GHz. The integration process is illustrated in the Extended Data Figure S10. First, MoS_2 phase-junction diode arrays were fabricated on a Kapton film following the above-mentioned processes. The G-S-G device configuration allows high frequency S-parameter measurements. The MoS_2 diode was subsequently cut off from the Kapton film in a roughly 0.5 mm x 1mm square patch. The Kapton square patch containing the MoS_2 diode was then flipped over and mounted on the receiver antenna in a face-to-face fashion. The MoS_2 diode and the receiver antenna were aligned under microscope in the way that the two terminals of signal line were electrically connected to the two transmission lines of the receiver antenna using conductive silver paste. The dimension of the G line (170 μm) is designed to be shorter than the gap between the antenna transmission lines (250 μm) to avoid shorting effect (Figure 3e). And the dimension of the signal line (1 mm) is designed to be larger than the gap between the antenna transmission lines (250 μm) to allow electrical connection. During the demonstration of energy harvesting, a commercial transmitter Wi-Fi band antenna was powered by a signal generator (Keysight N5183A) and approached the MoS_2 rectenna (Extended Data Figure S10b). The rectified output voltage V_{out} was measured by an oscilloscope with 1 MΩ impedance (Keysight DSO6054A). The rectenna was connected to an oscilloscope through an SMA connector. A load resistance of 10 KΩ is connected with the oscilloscope in a parallel configuration (Extended Data Figure S8), so the effective output resistance is about 10 kΩ. The available input power to the MoS_2 rectenna was about 3 dBm (~ 2 mW). The distance between our flexible rectenna and a commercial Wi-Fi band antenna (PCB Yagi antenna, 2 dBi gain), which is powered by a signal generator (continuous wave), is about 2.5 cm. The orientation of the MoS_2 rectenna was optimized, with respect to the used commercial Wi-Fi antenna, in order to maximize the collection of RF power.

S-parameter Measurement and Equivalent Circuit Modeling

In order to characterize the high frequency performance of our MoS_2 Schottky diode, we performed S-parameter measurements by using a vector network analyzer (Keysight N5230A). The two-channel microwave receiver allows us to measure the magnitude and phase of the transmitted and the reflected waves from the device. Two transmission line cables with 50 Ω impedance were connected to the device under test (DUT) through ground-signal-ground (G-S-G) probes. Proper calibration was done to eliminate the extrinsic effects and the systematic error of the measurement system[8]. The RF source was set to sweep from 100 MHz and 20 GHz, and an internal reflectometer was used to detect the incident, reflected and transmitted RF waves. The magnitude and phase of S_{11}, S_{21}, S_{12}, S_{22} were measured and recorded (Figure 2b, 2c & Extended Data Figure S4). The S_{11} represents the reflection coefficient at the input port, while S_{22} represents the reflection coefficient at its output port. The S_{21} is a measure of the insertion loss of the DUT, and the S_{12} characterizes the isolation from the output to the input. The S-parameter measurements were repeated when the DUT was biased at different bias points from -0.6V to 3V. The S-parameters were measured when the MoS_2 Schottky diode was under non-bending conditions.

To gain further insight into the capacitive and resistive components of the MoS_2 diode, we built a small-signal equivalent circuit to model the device by using Keysight's Advanced Design System (ADS). The schematic of the simulation circuit is shown in Figure 2a. The internal part of the MoS_2 diode was modeled by the series resistance R_s, the nonlinear junction resistance R_j and the junction capacitance C_j. The series resistance R_s includes the Ohmic contact resistance of the diode. The junction resistance R_j represents the nonlinear resistance of the Schottky junction which is bias-dependent. The junction capacitance of the diode is represented by C_j and it is also bias-dependent. The external parasitics of the MoS_2 diode are also considered and analyzed: C_f denotes the fringing capacitance between the diode's anode and cathode metal pads. The C_p incorporates the parasitic capacitance between the electrodes of the diode and the ground plane (Figure 2a). A quasi-Newton algorithm was used to optimize the parameters of the model. As illustrated in Figure 2b and 2c and Extended Data Figure S4, the simulated S-parameters match well the measured S-parameters.

The series resistance R_s and the junction resistance R_j can be obtained from the experimental S-parameters (Extended Data Figure S5). Figure S5a shows the R_s as a function of the applied bias. The series resistance R_s slightly increases from 2400 Ω to 3400 Ω as the applied bias increases from -0.6V to 3V. The semiconducting MoS_2 region incorporates two parts: depletion region and quasi-neutral region (i.e. regions without band bending). As the bias increases, the depletion region of MoS_2 will shrink, which can be seen from the conventional depletion thickness formula[25] in a Schottky diode $x_d = \sqrt{\frac{2\epsilon(\phi_{bi}-V)}{eN_d}}$, where ϵ is the permittivity of MoS_2, ϕ_{bi} is the built-in potential, V is the applied bias, e is electron charge, and N_d is the doping level of MoS_2. As the depletion

region of MoS_2 shrinks, the quasi-neutral region of MoS_2 therefore expands and contributes to an increased series resistance R_s. The junction resistance R_j decreases as the diode is turned on (Extended Data Figure S5b). The R_s and R_j obtained from S-parameter measurements are also confirmed by quasi-static IV measurement and modeling (Extended Data Figure S6). Similarly, the junction capacitance C_j can be extracted from the measured S-parameters. Figure 2d summarizes the evolution of C_j at different internal biases. The internal bias V_{int} is the voltage dropped across the nonlinear junction resistance R_j only and it can be calculated as $V_{int} = V_{ext} - I \cdot R_s$, where V_{ext} is the total bias applied across the MoS_2 diode. The junction capacitance of a Schottky diode can be modeled by Equation (3). As shown in Figure 2d, in the low-bias region (V<0.4V), the junction capacitance C_j of the MoS_2 diode is in the sub-10 fF regime (device width: 40μm). We attribute this ultralow junction capacitance of the device to its lateral structure. In such a lateral device structure, the charge transport across the Schottky barrier mainly occurs near the MoS_2 phase boundary with an extension within a transfer length scale λ, which is less than 1 μm[24,31]. Transfer length λ is the distance beyond which the current density drops by 1/e [25]. In other words, the applied bias will mainly drop across the region near the MoS_2 phase boundary, and therefore the modulation of the depletion region of MoS_2 will also mainly occurs within a transfer length scale. Consequently, it significantly reduces the effective area of the Schottky junction and thus the junction capacitance C_j. From Figure 2d, the built-in potential Φ_{bi} of the MoS_2-Pd Schottky junction can be extracted to be about 0.78eV based on Equation (3). The extrinsic parasitics can also be obtained based on the equivalent circuit modeling (Figure 2a Bottom): the fringing capacitance C_f is about 10 fF, and the parasitic capacitance C_p is about 20 fF. Thanks to the lateral design of our MoS_2 rectifier, the total capacitance of the device is about $C_f + C_p + C_j \sim 40$ fF (when one terminal of the circuit in Figure 2a is grounded). This value is about one order of magnitude smaller than state-of-the-art flexible rectifiers[9–12]. This is also confirmed by C-V measurements (Extended Data Figure S7).

RF-DC Power Conversion Efficiency and Wi-Fi band Energy Harvesting

At 2.4 GHz, the power efficiency of our flexible MoS_2 rectifiers is in the range of 10% - 40% for input power level between -15 dBm and 5 dBm (Figure 3b). As a proof-of-concept demonstration, our MoS_2 rectifiers exhibit competitive power efficiency. For comparison, the state-of-the-art rigid Si and GaAs Schottky diodes can exhibit power efficiency of 5% - 70% at the same frequency and the same range of input power level (Extended Data Figure S9). The maximum power efficiency η_{max} of our MoS_2 rectifiers at 2.4 GHz happens around the input RF power of -0.7 dBm ($\eta \sim 40.1\%$). The ambient Wi-Fi power collected by a 2.4 GHz Wi-Fi antenna is $P_{in} = W_s \cdot A_{eff} = (P_{TX} \cdot G_{TX} / 4\pi / d^2) \cdot (G_{RX} \cdot \lambda^2/4\pi) = [1\ W / 4\pi / (100\ cm)^2] \cdot [1.58 \times (12.5\ cm)^2/4\pi] \sim 156\ \mu W$ (i.e. -8 dBm), where the P_{in} is the input power to the receiver antenna, W_s is the ambient Wi-Fi power density, A_{eff} is the effective receiver antenna area, P_{TX} is the total power of transmitter antenna, G_{TX} is the transmitter antenna gain, d is the distance to the transmitter antenna (assuming 1m distance), G_{RX} is the receiver antenna gain (~ 2 dBi in our flexible antenna design, i.e. power ratio of 1.58) and λ is the wavelength[32]. Please note that $P_{TX} \cdot G_{TX}$ is the equivalent isotropically radiated power (EIRP), and we use 1 W as a typical EIRP value for 2.4 GHz Wi-Fi transmitter antenna. For example, in the United States, the EIRP (2.4 GHz) is 1W[33]. It may vary from different regions in the world. At 2.4 GHz, the power efficiency of our MoS_2 device is about 31% (at P_{in} = -8 dBm, see Figure 3b). Therefore, even as a proof-of-concept demonstration, the output DC power of our MoS_2 phase hetero-junction based rectifier reached about $P_{out} = P_{in} \times \eta = 156\ \mu W \times 31\% = 48.4\ \mu W$ at the input power level of -8 dBm (at 2.4 GHz). Please note that this level of output power has been achieved in an academic environment without careful optimization. In our current MoS_2 device with channel width W of 40 μm, the maximum power efficiency (~ 40.1%) happens at input power level of -0.7 dBm. Based on microwave theory, the maximum power efficiency η_{max} point can be shifted to lower input power level (e.g. -8 dBm) by reducing the device area[34], which in our case is the channel width. Given a relatively large channel width (W = 40 μm) used in our current design, there is a large room of reducing the channel width and tuning the η_{max} point to lower power level. By shifting the η_{max} to -8 dBm, we can potentially harvest an output DC power of 156 μW × 40.1% = 62.6 μW out of the ambient Wi-Fi band energy. Through a joint optimization of the material engineering, phase-change process and matching circuit, the power efficiency of the presented MoS_2 phase-junction-based rectifiers can be further improved.

Theory of nonlinear diode rectification

A diode is a two-terminal electronic device with nonlinear I-V characteristics. The nonlinearity is the foundation for many useful applications, such as rectification, detection and frequency mixing[8]. The DC I-V characteristics of a Schottky diode can be modeled by $I(V) = I_s (e^{\alpha V}-1)$, where $\alpha = q/nk_BT$, I_s is the reverse saturation current, k_B is the Boltzmann constant, T is the temperature, q is the electron charge and n is the ideality factor. In a small-signal model, the I(V) can be expanded in Taylor series at $V=V_0$:

$$I(V) = I_0 + \Delta V \left.\frac{dI}{dV}\right|_{V=V_0} + \frac{1}{2}\Delta V^2 \left.\frac{d^2I}{dV^2}\right|_{V=V_0} + \cdots \quad (5)$$

, where $I_0 = I(V_0)$ and $\Delta V = V-V_0$.

In a small-signal approximation, we can denote the input voltage as

$$V = V_0 + A\cdot\cos(\omega t) \quad (6)$$

, where A is the amplitude of the microwave input signal. Plugging (6) into (5), the diode current becomes

$$I = I_0 + A\cos(\omega t)\left.\frac{dI}{dV}\right|_{V=V_0} + \frac{1}{2}A^2\cos^2(\omega t)\left.\frac{d^2I}{dV^2}\right|_{V=V_0} + \cdots = I_0 + \frac{1}{4}A^2\left.\frac{d^2I}{dV^2}\right|_{V=V_0} + A\cos(\omega t)\left.\frac{dI}{dV}\right|_{V=V_0} + \frac{1}{4}A^2\cos(2\omega t)\left.\frac{d^2I}{dV^2}\right|_{V=V_0} + \cdots$$

(7)

It can be seen from the above expression that the output signal contains DC components, RF signals with frequency ω and 2ω (as well as other higher order harmonics). The rectified DC current I_{DC} is the second term: $\frac{1}{4}A^2\left.\frac{d^2I}{dV^2}\right|_{V=V_0}$.

The intrinsic current responsivity R_i is defined as the ratio of the rectified DC current I_{DC} and the RF power delivered to the nonlinear junction resistance P_{in}. The P_{in} can be obtained from the time averaged integration of $\frac{1}{T}\int_0^T I(t)V(t)dt = \frac{1}{2}A^2\left.\frac{dI}{dV}\right|_{V=V_0}$.

Therefore, $R_i = \frac{I_{DC}}{P_{in}} = \left.\frac{d^2I}{dV^2}\right|_{V=V_0} \Big/ 2\cdot\left.\frac{dI}{dV}\right|_{V=V_0}$

In the calculation of the intrinsic responsivity in Figure 1c, Savitzky-Golay Smoothing method was used to take average of the slopes in 10 points of window.

Analysis of the cutoff frequency f_c

In this work, the cutoff frequency of a high-speed diode is defined by the conventional "-3dB point", which is different from the cutoff frequency defined for traditional transistors (*i.e.* unit gain point). Here we explain in details how the cutoff frequency f_c of MoS_2 Schottky diode is defined. The internal part of a Schottky diode can be modeled by a series resistance R_s, a junction resistance R_j and a junction capacitance C_j, as indicated by Figure 2a. Let us denote the total voltage applied across the intrinsic diode as V and denote the voltage across R_j as V_j. The overall impedance of the diode is represented by Z. Then the RF power absorbed by the diode can be calculated as[26]

$$P_{RF} = \frac{|V|^2}{2}\mathrm{Re}\{\frac{1}{Z}\} \quad (8)$$

, where $Z = R_s + \frac{1}{\frac{1}{R_j} + j\omega C_j}$. Plugging Z into (8), we can get

$$P_{RF} = \frac{|V|^2}{2} \cdot \frac{\frac{1}{R_j}(1+\frac{R_s}{R_j}) + \omega^2 C_j^2 R_s}{(1+\frac{R_s}{R_j})^2 + \omega^2 C_j^2 R_s^2} \quad (9)$$

The voltage across R_j can be calculated as

$$|V_j|^2 = |V|^2 \left| \frac{\frac{1}{\frac{1}{R_j} + j\omega C_j}}{\frac{1}{\frac{1}{R_j} + j\omega C_j} + R_s} \right|^2 = |V|^2 \left| \frac{1}{1+\frac{R_s}{R_j} + j\omega C_j R_s} \right|^2 = \frac{|V|^2}{\left(1+\frac{R_s}{R_j}\right)^2 + \omega^2 C_j^2 R_s^2} \quad (10)$$

Therefore, P_{RF} can be expressed in terms of V_j as follows:

$$P_{RF} = \frac{|V|^2}{2} \cdot \frac{\frac{1}{R_j}(1+\frac{R_s}{R_j}) + \omega^2 C_j^2 R_s}{(1+\frac{R_s}{R_j})^2 + \omega^2 C_j^2 R_s^2} = \frac{|V_j|^2}{2}\left[\frac{1}{R_j}\left(1+\frac{R_s}{R_j}\right) + \omega^2 C_j^2 R_s\right] \quad (11)$$

The part of the incident power consumed by R_j is

$$P_j = \frac{|V_j|^2}{2R_j} \quad (12)$$

So

$$\frac{P_j}{P_{RF}} = \frac{1}{1+\frac{R_s}{R_j} + \omega^2 C_j^2 R_s R_j} = \frac{1}{\left(1+\frac{R_s}{R_j}\right) \cdot \left[1+\frac{\omega^2 C_j^2 R_s R_j}{1+\frac{R_s}{R_j}}\right]} \quad (13)$$

By defining the cutoff frequency f_c as the frequency at which P_j/P_{RF} is half of its value at DC (*i.e.* -3dB point), we have

$$\frac{P_j}{P_{RF}} = \frac{1}{\left(1+\frac{R_s}{R_j}\right)\left[1+\left(\frac{f}{f_c}\right)^2\right]} \quad (14)$$

By using this "-3dB point" definition, f_c can be obtained as:

$$f_c = \frac{\sqrt{1+\frac{R_j}{R_s}}}{2\pi R_j C_j} \quad (15)$$

Extended Data

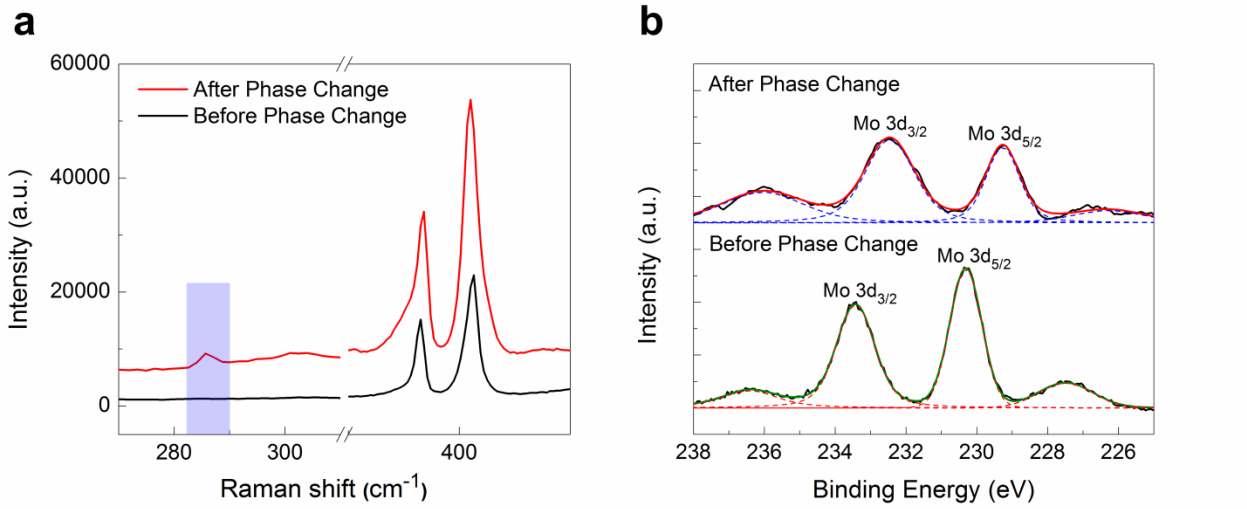

Extended Data Figure S1. Spectroscopic study of MoS_2 before and after phase change induced by n-Butyllithium. (a) The Raman spectrum of MoS_2 before and after the phase change induced by n-Butyllithium. A new Raman peak around 286 cm^{-1} was developed after the phase change. (b) The XPS characterization of MoS_2 samples (Mo $3d_{3/2}$ and Mo $3d_{5/2}$ peak) before and after the 2H to 1T/1T' phase change induced by n-Butyllithium. The Mo $3d_{3/2}$ and Mo $3d_{5/2}$ peak experienced red shift after the phase change.

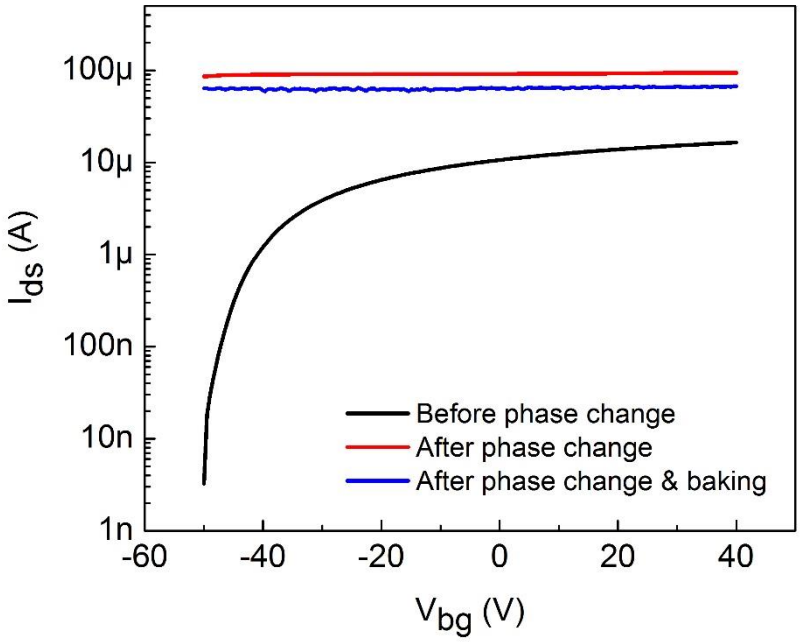

Extended Data Figure S2. IV transfer characteristics of MoS_2 field effect transistor (FET) on a Si wafer capped with 300nm SiO_2, before and after phase change (drain current as a function of backgate bias, drain voltage V_{ds} = 50mV, channel length = 830nm, channel width = 50µm). The 300nm SiO_2 serves as the backgate dielectric layer. Black line: pristine MoS_2 FET; Red line: MoS_2 FET after phase change through n-butyl lithium treatment. Blue line: after baking (180 ˚C for 3min) of post-phase-change MoS_2 FET. The 1T phase MoS_2 is unstable in the air at room temperature, and part of the 1T region will convert into 1T' phase. However, the 1T/1T' mixture MoS_2 remains metallic IV characteristics after baking.

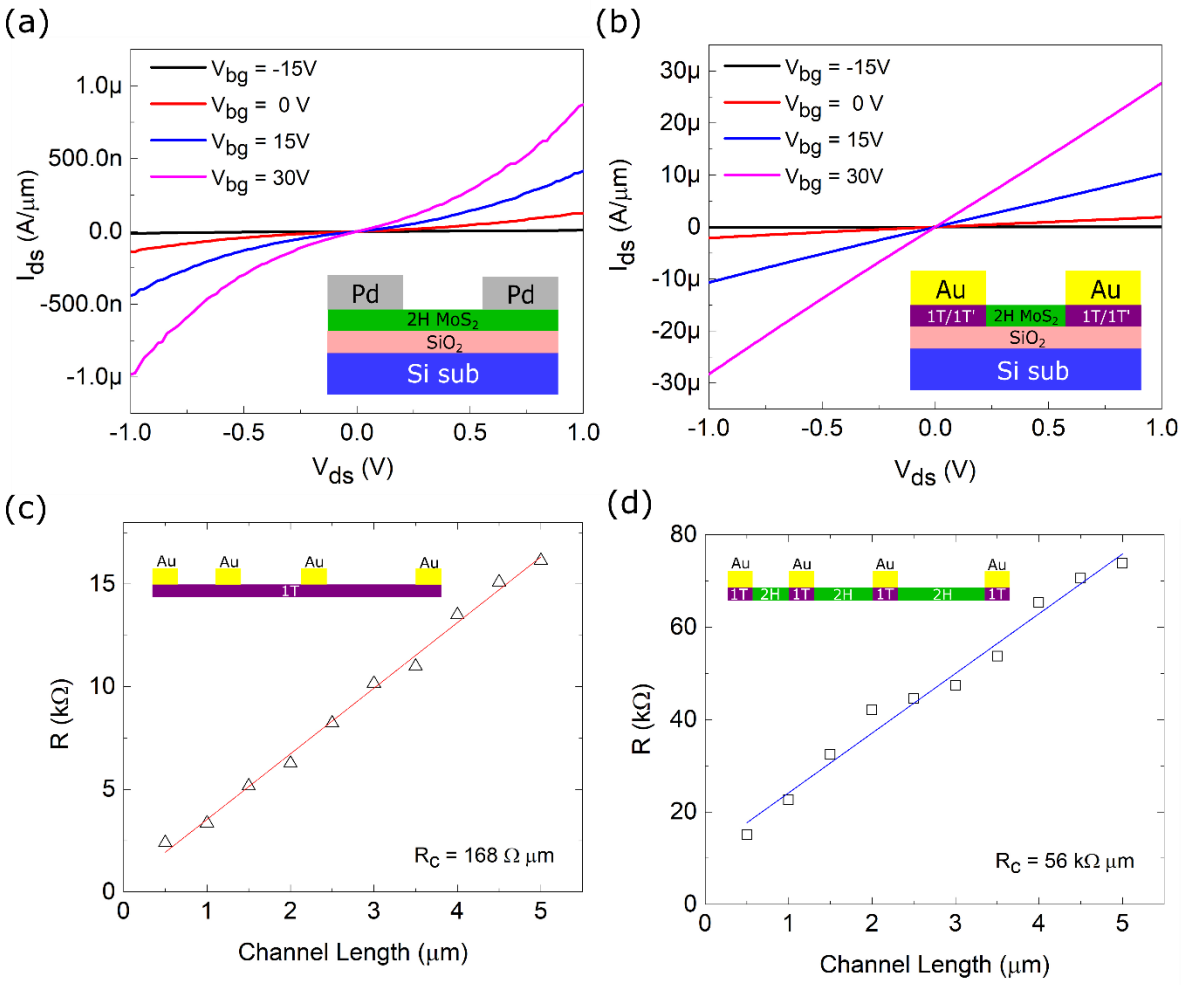

Extended Data Figure S3. Investigation of Schottky contact in Pd/2H MoS_2 and Ohmic contact in Au/1T MoS_2/2H MoS_2. (a) IV characteristics of backgated MoS_2 transistors on Si substrates capped with 300nm SiO_2. Channel length: 4μm. Pd was used as source/drain contact metal. The nonlinear I_{ds}-V_{ds} characteristics show Schottky contact behavior. (b) IV characteristics of backgated MoS_2 transistors on Si substrates capped with 300nm SiO_2. Channel length: 4μm. The source/drain region of MoS_2 was phase-engineered into metallic 1T/1T' phase as contact. The linear I_{ds}-V_{ds} characteristics show Ohmic contact nature. (c) Transfer length method (TLM) structure of 1T/1T' MoS_2. The contact resistance between Au and 1T/1T' MoS_2 was estimated to be about 168 Ω·μm. (d) TLM structure of 2H MoS_2, in which the contact area was phase-engineered into 1T/1T' metallic phase before metal deposition. The contact resistance was estimated to be 56 kΩ·μm.

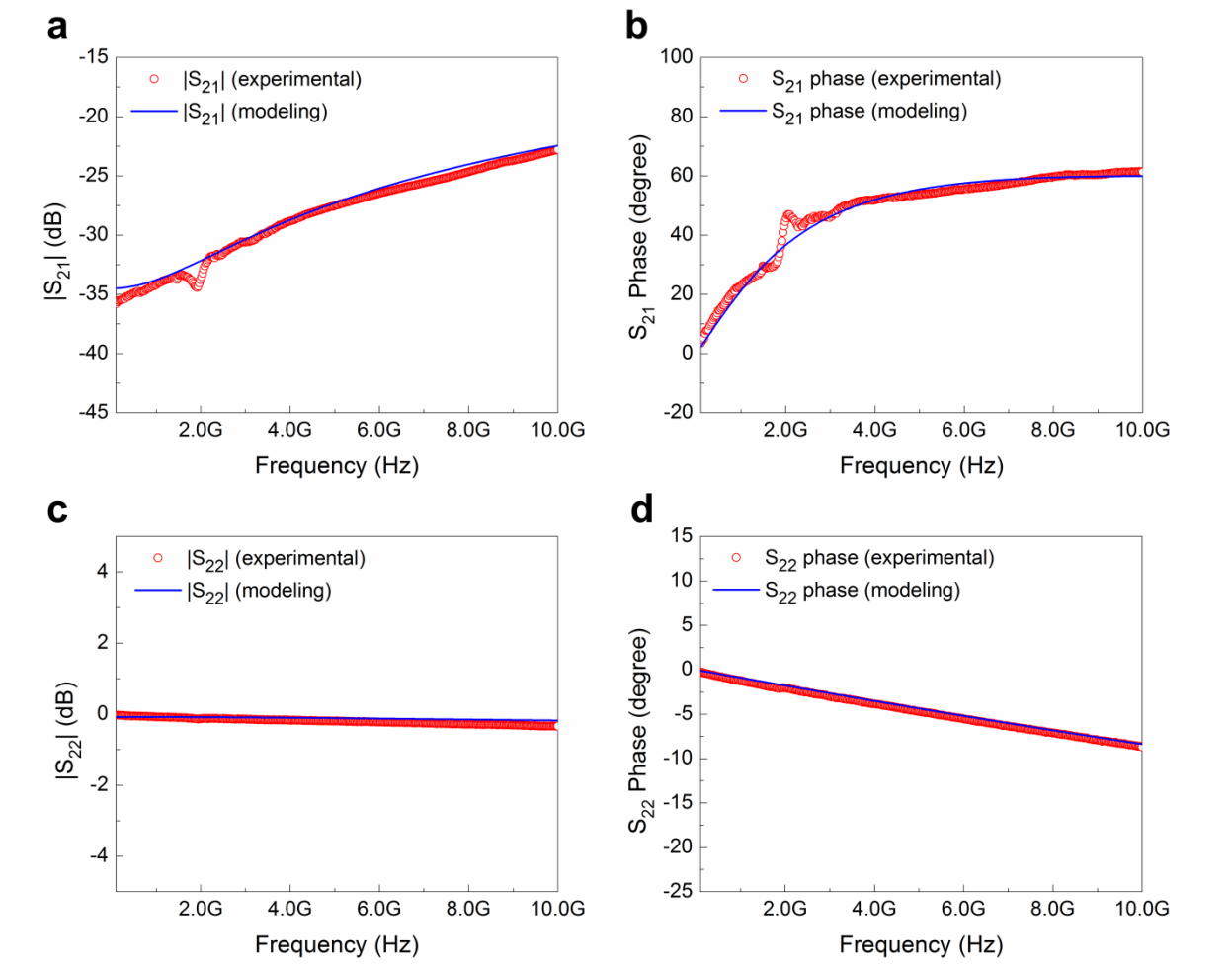

Extended Data Figure S4. The comparison of the measured S-parameter of the MoS_2 diode and the modeled S-parameter based on the equivalent circuit in Figure 2a. Red open circles: experimental data; Blue line: modeling. (a) The magnitude of S_{21}. (b) The phase of S_{21}. (c) The magnitude of S_{22}. (d) The phase of S_{22}.

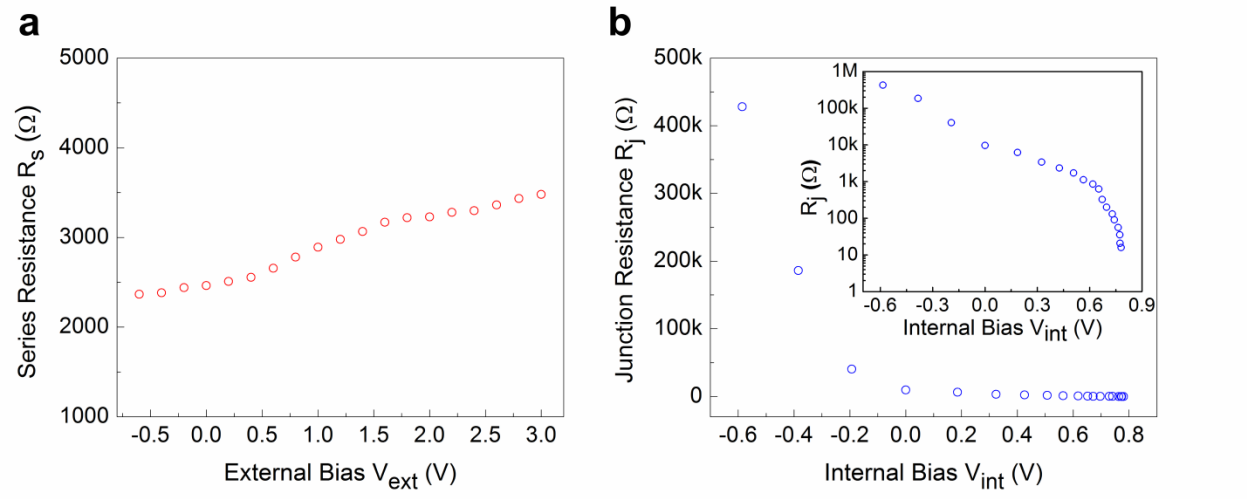

Extended Data Figure S5. The series resistance R_s and junction resistance R_j obtained from S-parameter measurements. (a) The series resistance R_s obtained from S-parameter at different external bias. (b) The junction resistance R_j obtained from S-parameter at different internal bias. The internal bias V_{int} is derived from $V_{int} = V_{ext} - I \cdot R_s$.

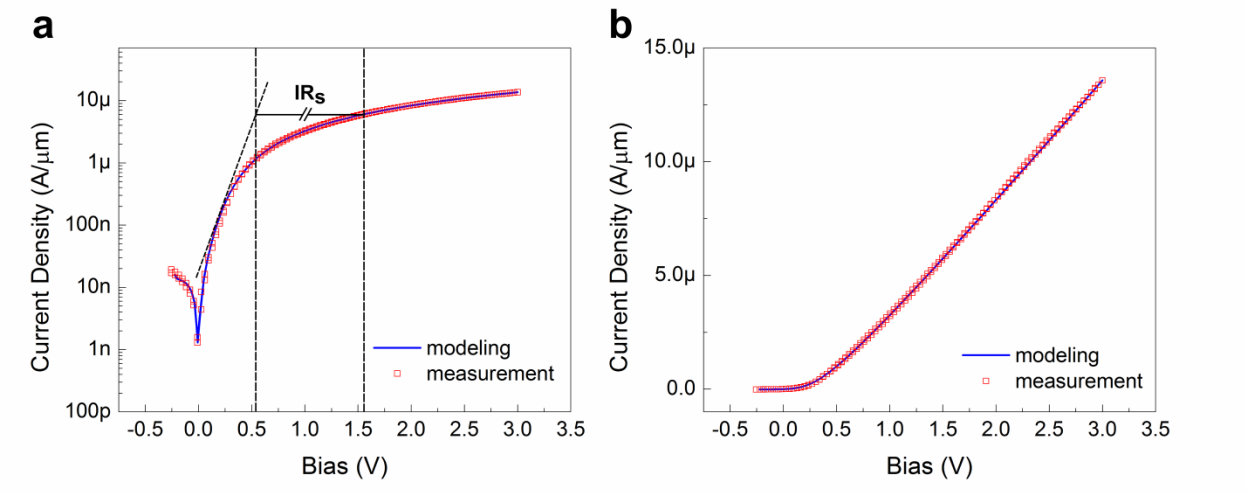

Extended Data Figure S6. The quasi-static I-V characteristics of the MoS_2 Schottky diode. The modeling is based on $I = I_s [\exp(q(V-IR_s)/nk_BT]-1]$, where k_B is the Boltzmann constant, I_s = 700 nA, n = 2.9, R_s = 3500 Ω, T = 300 K. (a) The current density of MoS_2 phase-junction diode in log scale. (b) The current density of MoS_2 phase-junction diode in linear scale (blue line: modeling; red open square: measurements).

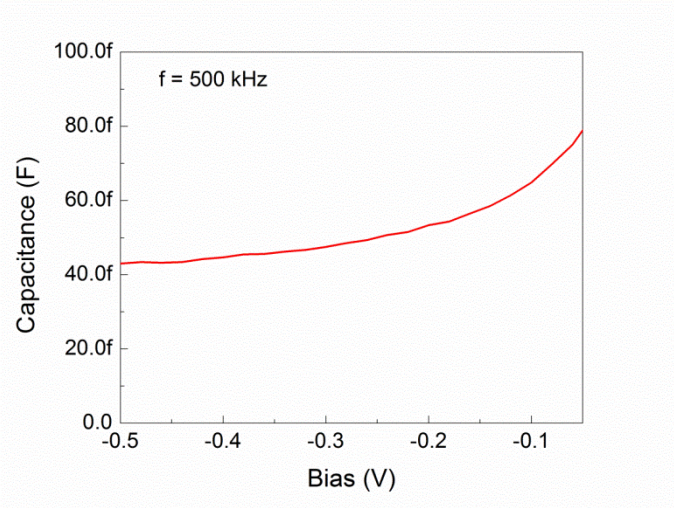

Extended Data Figure S7. The C-V characteristics of the MoS_2 Schottky diode measured at f = 500 kHz (Keysight 1500B)**.** When the MoS_2 diode is negatively biased or around zero bias, the overall capacitance is about 40-60 fF. This result is roughly consistent with the capacitive components obtained from high-frequency S-parameter measurements. From S-parameter measurements, the fringing capacitance C_f is about 10 fF, and the parasitic capacitance C_p is about 20 fF. The total capacitance of our MoS_2 Schottky diode is about $C_f + C_p + C_j \sim 40$ fF (when one terminal of the equivalent circuit in Figure 2a is grounded).

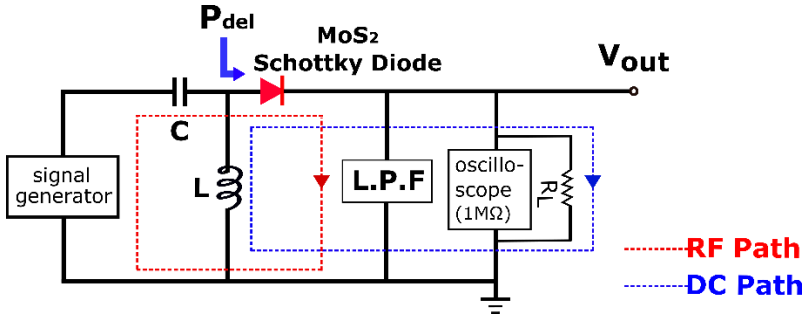

Extended Data Figure S8. Circuit diagram of the MoS_2–based RF energy harvester circuit. The decoupling capacitors at the input can block the DC current while permitting passage of RF signals. The DC and RF signal paths are indicated by blue and red dash lines, respectively. The output signal was measured by an oscilloscope with a 1MΩ impedance (Keysight DSO6054A), which is in shunt with a load resistance. The capacitor in this circuit is to block DC current and protect the signal generator, and it is not necessary for demonstration using antenna.

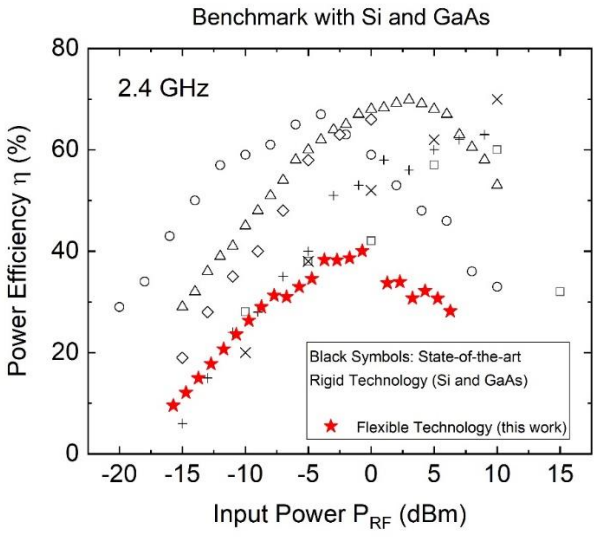

Extended Data Figure S9. Power efficiency of MoS_2 phase-junction based rectifiers and the benchmark with the state-of-the-art rigid technologies at 2.4 GHz (Si Schottky diodes and GaAs Schottky diodes). Data in black symbols are from references[35–40]. To ensure a fair comparison, all the data points here are the RF-DC conversion efficiency for rectifiers without antenna effect. As a proof-of-concept demonstration, the flexible MoS_2 rectifiers exhibit competitive power efficiency. Please note that the power efficiency has been obtained in an academic environment without careful optimization. Through a joint optimization of the material engineering, phase-change process and matching circuit, the power efficiency of the presented MoS_2 phase-junction-based rectifiers can be further improved. Moreover, the flexibility of the MoS_2 rectifiers is a critical advantage compared with rigid technologies, because it could enable electronics with new form factors that allow seamless integration with objects in arbitrary shapes.

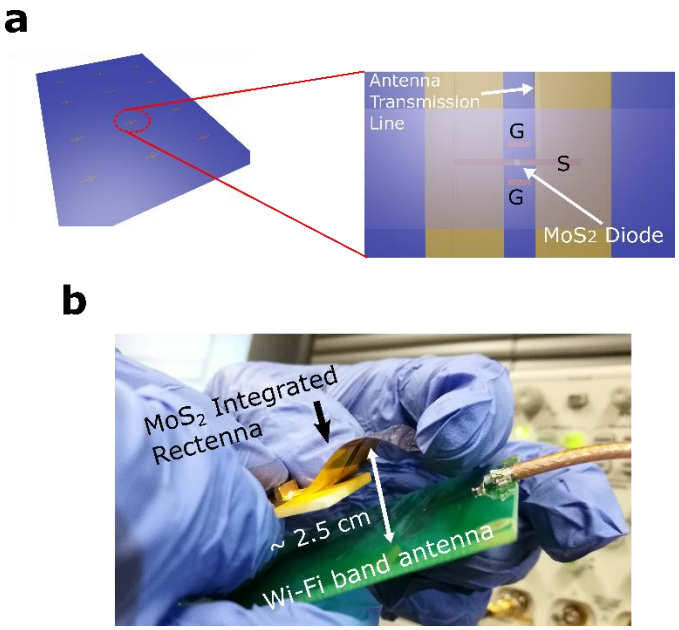

Extended Data Figure S10. Integration of fully flexible MoS_2 rectenna harvesting the electromagnetic radiation energy in the Wi-Fi band (5.9 GHz). (a) Fabrication process of integrated MoS_2 rectenna on flexible Kapton substrates. The phase engineered MoS_2 rectifier arrays are fabricated on Kapton substrates. After high-frequency characterization by S-parameter measurements, we integrated the MoS2 rectifier with a flexible 5.9 GHz Wi-Fi antenna on the same piece of Kapton film. The dimension of the G line (170 μm) is designed to be shorter than the gap between the antenna transmission lines (250 μm) to avoid shorting effect. The dimension of the signal line (1 mm) is designed to be larger than the gap between the antenna transmission lines (250 μm) to allow connection. (b) Demonstration of energy harvesting of EM radiation in the 5.9 GHz Wi-Fi band using the as-fabricated flexible MoS_2 rectenna. The available input power to the MoS_2 rectenna is about 3 dBm (~2 mW). The measurement is carried out in a parallel configuration (as shown in Figure 3d). A transmitter Wi-Fi band antenna is powered by a signal generator (Keysight N5183A) and approached the receiver antenna of MoS_2 rectenna. The rectified output voltage V_{out} is about 250 mV, which is measured from an oscilloscope (Keysight DSO6054A) in shunt with a 10 kΩ load resistance. The power transmission efficiency can be further improved by optimizing the impedance matching between the receiver antenna and MoS_2 diode.

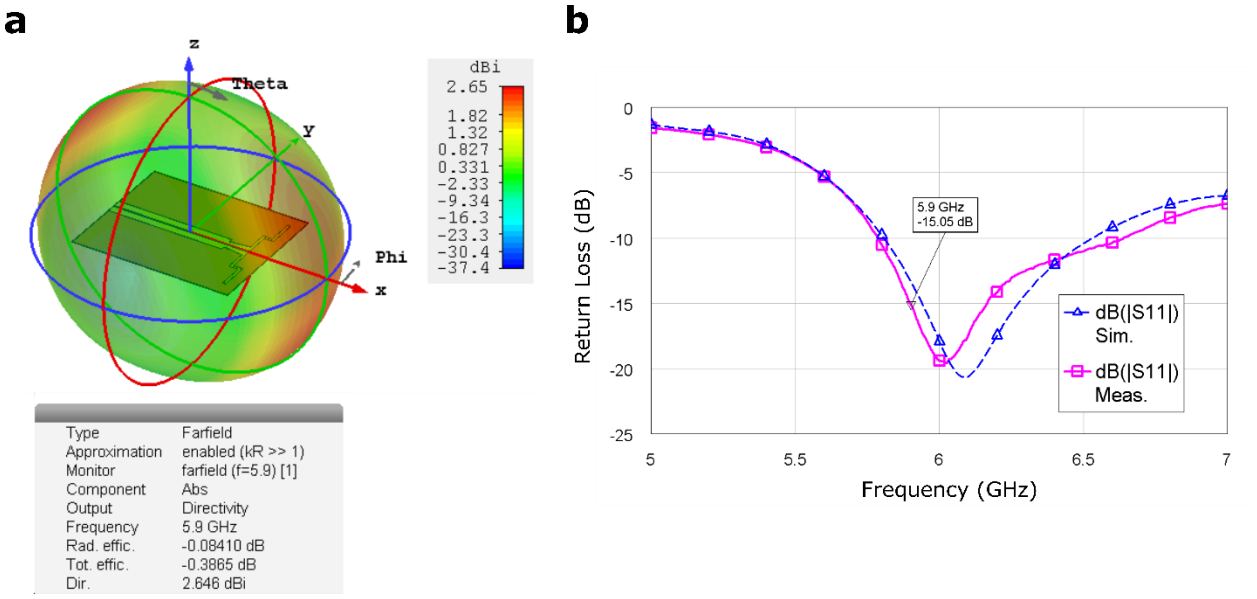

Extended Data Figure S11. Simulation and characterization of the flexible Wi-Fi band antenna fabricated on Kapton. (a) Simulated directivity pattern of the flexible dipole antenna including the feeding line effect. The total antenna gain is expected to be only -0.38 dB below the directivity (D_0 = 2.64 dB) due to the low Ohmic loss and the very good impedance matching with respect to 50 Ohm that is observed in (b) for both simulations and measurements at the operating frequency.

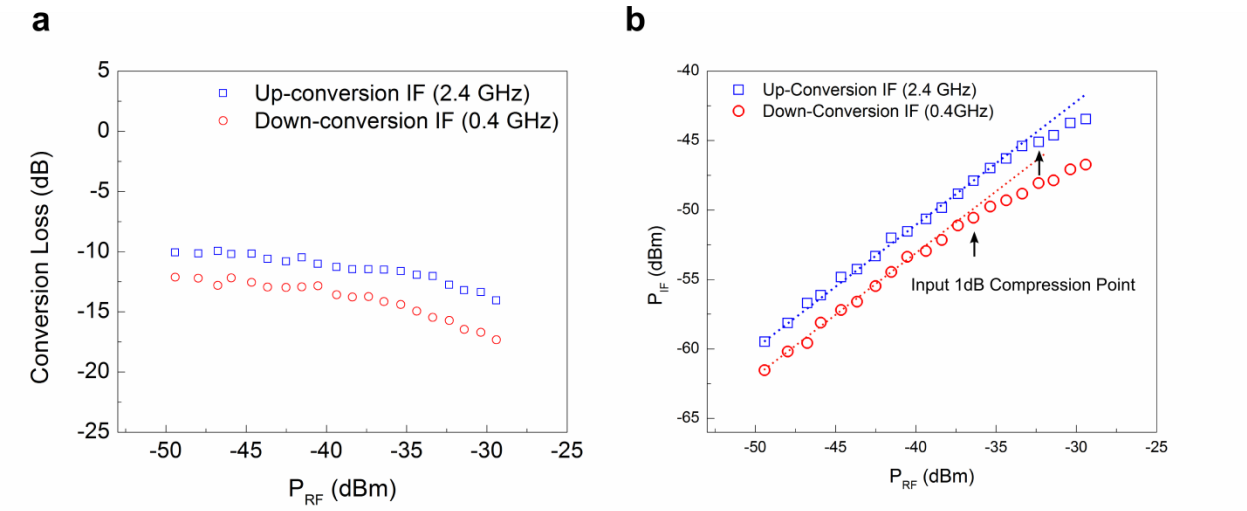

Extended Data Figure S12. (a) Conversion loss of the MoS_2 mixer at different delivered RF power at the input. The conversion loss is defined as the power difference between input RF signal (1.4 GHz) and output IF (down-converted 0.4 GHz and up-converted 2.4 GHz). (b) Input 1 dB compression point of MoS_2 mixer. The 1 dB compression point is a measure of an RF mixer's linearity and it is defined as the input RF power where the conversion loss is increased by 1 dB from ideal. For the up-conversion IF 2.4 GHz, the 1dB point compression point is about -32.3 dBm. For the down-converted IF 0.4 GHz, the 1dB point compression point is about -36.4 dBm.

Extended Data Table S1. Comparison of state-of-the-art gigahertz flexible rectifiers in terms of cutoff frequency f_c, mobility and Rigidity.

	Materials	Highest f_c (GHz) (defined as -3dB point)	Mobility ($cm^2V^{-1}s^{-1}$)	Maximum Elastic Strain Limit	References
Flexible Technology	MoS_2	10	10-100	23 %	This work, 2, 41
	IGZO	1	1-50	2.9 %	9,10,12,42,43
	Amorphous Silicon	1.6	1-10	5 %	11,44,45
	Organic semiconductor (Pentacene)	0.87	0.001-1	10 %	3,17,46,47
Rigid Technology	Single Crystalline Silicon	400	1400	0.3 %	48, 49

31. Guo, Y. *et al.* Study on the Resistance Distribution at the Contact between Molybdenum Disulfide and Metals. *ACS Nano* **8,** 7771–7779 (2014).
32. Mou, J., Xue, Q., Guo, D. & Lv, X. A THz Detector Chip With Printed Circular Cavity as Package and Enhancement of Antenna Gain. *IEEE Trans. Antennas Propag.* **64,** 1242–1249 (2016).
33. Maximum wifi transmission power per country. *Wolph* (2015).
34. Grajal, J., Krozer, V., Gonzalez, E., Maldonado, F. & Gismero, J. Modeling and design aspects of millimeter-wave and submillimeter-wave Schottky diode varactor frequency multipliers. *IEEE Trans. Microw. Theory Tech.* **48,** 700–711 (2000).
35. Valenta, C. R. & Durgin, G. D. Harvesting Wireless Power: Survey of Energy-Harvester Conversion Efficiency in Far-Field, Wireless Power Transfer Systems. *IEEE Microw. Mag.* **15,** 108–120 (2014).
36. Mbombolo, S. E. F. & Park, C. W. An improved detector topology for a rectenna. in *2011 IEEE MTT-S International Microwave Workshop Series on Innovative Wireless Power Transmission: Technologies, Systems, and Applications* 23–26 (2011).
37. Olgun, U., Chen, C. & Volakis, J. L. Investigation of Rectenna Array Configurations for Enhanced RF Power Harvesting. *IEEE Antennas Wirel. Propag. Lett.* **10,** 262–265 (2011).
38. Olgun, U., Chen, C. & Volakis, J. L. Wireless power harvesting with planar rectennas for 2.45 GHz RFIDs. in *2010 URSI International Symposium on Electromagnetic Theory* 329–331 (2010).
39. Wang, D. & Negra, R. Design of a rectifier for 2.45 GHz wireless power transmission. in (VDE, 2012).
40. Kim, J. & Jeong, J. Design of high efficiency rectifier at 2.45 GHz using parasitic canceling circuit. *Microw. Opt. Technol. Lett.* **55,** 608–611 (2013).
41. Bertolazzi, S., Brivio, J. & Kis, A. Stretching and Breaking of Ultrathin MoS2. *ACS Nano* **5,** 9703–9709 (2011).

42. Kwon, J.-Y., Lee, D.-J. & Kim, K.-B. Review paper: Transparent amorphous oxide semiconductor thin film transistor. *Electron. Mater. Lett.* **7,** 1–11 (2011).

43. Mohammed, D. W. *et al.* Mechanical properties of amorphous indium–gallium–zinc oxide thin films on compliant substrates for flexible optoelectronic devices. *Thin Solid Films* **594,** 197–204 (2015).

44. Freund, L. B. & Suresh, S. *Thin Film Materials: Stress, Defect Formation and Surface Evolution*. (Cambridge University Press, 2004).

45. Sun, J., Zhang, B. & Katz, H. E. Materials for Printable, Transparent, and Low-Voltage Transistors. *Adv. Funct. Mater.* **21,** 29–45 (2011).

46. Shaw, J. M. & Seidler, P. F. Organic electronics: Introduction. *IBM J. Res. Dev.* **45,** 3–9 (2001).

47. Tahk, D., Lee, H. H. & Khang, D.-Y. Elastic Moduli of Organic Electronic Materials by the Buckling Method. *Macromolecules* **42,** 7079–7083 (2009).

48. Contents Volume 23. *Mech. Mater.* **23,** 333–334 (1996).

49. Sankaran, S. & O, K. K. Schottky diode with cutoff frequency of 400 GHz fabricated in 0.18 mu;m CMOS. *Electron. Lett.* **41,** 506–508 (2005).